ON THE CLASSIFICATION OF SEA ICE TYPES USING SIMULATED RADARSAT CONSTELLATION MISSION (RCM) COMPACT POLARIMETRIC SAR PARAMETERS

M. Dabboor*, Postdoctoral researcher
T. Geldsetzer**, Research Scientist
*Science and Technology Branch, Environment Canada. 4905 Dufferin Street
Toronto, ON, Canada, M3H 5T4.
Mohammed.Dabboor@ec.gc.ca
**1633 Broadview Rd. NW, Calgary, Alberta, Canada, T2N 3H2.
Torsten.Geldsetzer@gmail.com

ABSTRACT

A Synthetic Aperture Radar (SAR) system with hybrid-polarity architecture constitutes a significant advancement in the field of radar remote sensing. This new architecture system is a Compact Polarimetric (CP) SAR system which transmits a circular polarization and receives two mutually coherent orthogonal linear polarizations. This SAR system reduces some of the design constraints of the spaceborne satellite, allowing for a low-cost and low-mass SAR system. The main advantage of this SAR system is that it has a greater amount of information than the standard dual-pol mode, while covering the swath width of ScanSAR imagery. Therefore, a growing interest has been raised for CP SAR systems as a possible tradeoff in full quad-pol SAR systems. A CP SAR mode will be included in future SAR missions, such as the Canadian RADARSAT Constellation Mission (RCM) and the Japanese Advanced Land Observing Satellite-2 (ALOS-2). This paper is a first attempt towards the selection of the optimum CP parameters for sea ice classification. A set of twenty three CP parameters are assessed. A late-winter case study image is used, encompassing two sea ice types and one open water state.

KEYWORDS: Compact SAR; RADARSAT Constellation Mission; Sea ice Classification

INTRODUCTION

Synthetic Aperture Radar (SAR) sea ice classification and mapping at operational scales usually relies on single- or dual-polarized imagery. However, such imagery is limited in its ability to discriminate certain sea ice types and open water states (Geldsetzer and Yackel, 2009). The additional information contained in polarimetric SAR imagery may be used to improve classification potential (e.g. Gill and Yackel, 2012), but current image swath widths (up to 50 km for RADARSAT-2 quad-pol-wide) are too small for operational application.

A SAR system with hybrid-polarity architecture constitutes a significant advancement in the field of radar remote sensing (Raney, 2007). Such architecture is included in the current Indian RISAT-1 satellite, and it will be included in future SAR missions, such as the Canadian RADARSAT Constellation Mission (RCM), and the Japanese Advanced Land Observing Satellite-2 (ALOS-2). The main advantage of such SAR systems is that they have a greater amount of information than standard dual-pol mode, while covering much greater swath widths compared to quad-pol mode. RCM will transmit a right-circular polarization and receives two mutually coherent orthogonal linear polarizations (RH and RV), providing compact polarimetry (CP) as a primary imaging mode. CP parameters for sea ice discrimination have shown promise in preliminary studies (Charbonneau et al., 2010), and may have classification potential similar to that of fully polarimetric parameters. Furthermore, CP data will be available at swaths up to 500 km wide, making it operationally viable.

In this study, we investigate the potential of the future CP SAR system in the RCM satellite for sea ice type classification. We use simulated CP SAR parameters from thee CP RCM future modes with different resolutions and noise floors. The three different CP sets of parameters are separately used as input data for sea ice type identification through a Maximum Likelihood (ML) classification approach. Furthermore, we evaluate the three CP parameter sets for the discrimination between ice and open water (OW) areas. RADARSAT-2 data of sea ice collected over the Barrow Strait close to the Somerset Island in the Canadian Arctic are used.

METHODOLOGY

Different sets of CP SAR parameters can be calculated and used for sea ice classification. In this study, twenty three simulated CP SAR parameters are calculated and their potential for sea ice type discrimination is evaluated.

Table 1: The twenty-three simulated RCM compact polarimetric SAR parameters.

Symbol	Name	Formula
σ°_{RH}	Sigma naught backscatter value at indicated polarizations	$\sigma^{o} = g_{AR}^{T} * g_{R}$
σ°_{RV}	Sigma naught backscatter value at indicated polarizations	$\sigma^{o} = g_{AR}^{T} * g_{R}$
σ°_{RR}	Sigma naught backscatter value at indicated polarizations	$\sigma^{o} = g_{AR}^{T} * g_{R}$
σ°_{RL}	Sigma naught backscatter value at indicated polarizations	$\sigma^{o} = g_{AR}^{T} * g_{R}$
γ_{rvrh}	Circular cross polarization ratio	$\gamma_{rvrh} = \langle \sigma^{\circ}_{RV} \rangle / \langle \sigma^{\circ}_{RH} \rangle$
δ	Relative phase of *RV* and *RH*	Eq. (6) in (Charbonneau et al., 2010)
m	Degree of polarization	Eq. (3) in (Raney et al., 2012)
u	Conformity coefficient	Eq. (20) in (Truong-Loi et al., 2009)
ρ	Correlation coefficient of *RV* and *RH* (amplitude)	$\rho = \left\| \frac{\sqrt{\langle S_{RH} S_{RV}^{*} \rangle}}{\sqrt{\langle S_{RH} S_{RH}^{*} \rangle + \langle S_{RV} S_{RV}^{*} \rangle}} \right\|$
μ_c	Circular polarization ratio	Eq. (3) in (Charbonneau et al., 2010)
m-χ-e	Even bounce scattering based on m-chi decomposition	Eq. (5) in (Raney et al., 2012)
m-χ-v	Volume scattering based on m-chi decomposition	Eq. (5) in (Raney et al., 2012)
m-χ-o	odd scattering based on m-chi decomposition	Eq. (5) in (Raney et al., 2012)
m-δ-db	Double bounce scattering based on m-delta decomposition	Eq. (7) in (Charbonneau et al., 2010)
m-δ-v	Volume scattering based on m-delta decomposition	Eq. (7) in (Charbonneau et al., 2010)
m-δ-s	Surface scattering based on m-delta decomposition	Eq. (7) in (Charbonneau et al., 2010)
α-s	Alpha parameter related to the ellipticity of the compact scattered wave	Eq. (9) in (Cloude et al., 2012)
H_i	Shannon entropy – intensity component	$H_i = 2\log\left(\frac{\pi e \mathrm{Tr}(T_2)}{2}\right)$
H_p	Shannon entropy – polarimetric component	$H_P = \log\left(\frac{4\lvert T_2 \rvert}{\mathrm{Tr}(T_2)^2}\right)$
g_0	Stokes vector first component	Eq. (2) in (Raney et al., 2012)
g_1	Stokes vector second component	Eq. (2) in (Raney et al., 2012)
g_2	Stokes vector third component	Eq. (2) in (Raney et al., 2012)
g_3	Stokes vector fourth component	Eq. (2) in (Raney et al., 2012)

In addition, we assess the potential of the estimated CP SAR parameters for the discrimination between ice and no ice regions. Table 1 shows the considered simulated CP SAR parameters in this study.

In Table 1, g_R is the received Stokes vector resulting from an antenna transmitting right circular polarization, g_{AR} is the Stokes vector of the receiving antenna: for horizontal (*RH*) receiving g_{AR}^T = [1 1 0 0], for vertical (*RV*) receiving g_{AR}^T = [1 -1 0 0], for right-circular receiving g_{AR}^T = [1 0 0 -1], and for left-circular receiving g_{AR}^T = [1 0 0 1]. S_{RH} and S_{RV} denote the complex elements of the compact polarimetric scattering vector, T_2 is the 2x2 compact polarimetric coherency matrix and Tr denotes the matrix trace.

We calculate the twenty three simulated CP SAR parameters for three RCM modes: 1) Low Noise 100 m, −25 dB noise floor (LN25); 2) Low Resolution 100 m, −22 dB noise floor (LR22); and 3) Medium Resolution 50 m, −22 dB noise floor (MR22). Our purpose is to determine for each RCM mode those parameters which better classify different ice types and also accurately discriminate between Ice and OW regions. Since the calculated CP SAR parameters are correlated, we adopt a supervised Maximum likelihood (ML) classification approach using as input data all the possible subsets of the calculated CP SAR parameters. The ML classification approach calculates the probability $g_i(x)$ that a given n-dimensional data pixel x belongs to a specific class w_i, as follow (Richards, 1999):

$$g_i(x) = \ln p(w_i) - \frac{1}{2}\ln|\Sigma_i| - \frac{1}{2}(x - m_i)^T \Sigma_i^{-1}(x - m_i) \quad (1)$$

where $p(w_i)$ is the probability that class w_i occurs in the data and is assumed the same for all classes, Σ_i is the covariance matrix of the data in class w_i, and superscript T denotes the transpose operation. Each pixel is assigned to the class that has the highest probability (Richards, 1999).

Applying the ML classification approach for each RCM mode to all the possible subsets of the twenty three available CP SAR parameters implies the repetition of the classification approach thousands of times (2^{23}-1 classifications). In order to reduce the high number of classifications that need to be applied, we calculate the separability of the classes in each CP SAR parameter using the Jeffries-Matusita (JM) separability criterion, which takes values in the interval [0, 2]. The closer the value of the JM separability to zero the lower is the separability between classes. On the other hand, the closer the JM separability value to 2, the higher is the separability between classes. The JM separability can be calculated as follow (Swain and Davis, 1978)

$$J_{ij} = 2(1 - e^{-d_{ij}}) \quad (2)$$

where d_{ij} is the Bhattacharyya distance, defined as (Duda et al., 2000)

$$d_{ij} = -\ln\left\{\int \sqrt{p(x/w_i)\, p(x/w_j)}\, dx\right\} \quad (3)$$

where $p(x/w_i)$ and $p(x/w_j)$ are the conditional probability density functions of the random variable x, given the data classes w_i and w_j, respectively. The Bhattacharyya distance is a special case of the Chernoff distance, which has the following form for the multivariate normal distribution (Duda et al., 2000)

$$f_{ij}(b) = \frac{b(1-b)}{2}(m_j - m_i)^T\left[b\Sigma_i + (1-b)\Sigma_j\right]^{-1}(m_j - m_i) + \frac{1}{2}\ln\frac{|b\Sigma_i + (1-b)\Sigma_j|}{|\Sigma_i|^b|\Sigma_j|^{1-b}} \quad (4)$$

where b is an optimization parameter ($0 \le b \le 1$). According to Swain and Davis (1978), the optimal Chernoff distance can be obtained by finding the optimal value of the parameter b which minimizes the function

$$g(b) = e^{-f(b)} \quad (5)$$

The function $g(b)$ is a convex downward function on the interval [0, 1] of b with only one local minima which corresponds to the optimal value of b (Duda et al., 2000). Thus, the Bhattacharyya distance is a special case of the Chernoff distance in which the parameter b is assumed to be equal to 0.5. Thus, instead of the Bhattacharyya distance, we calculate the optimal JM separability criterion by using the Chernoff distance.

In order to reduce the number of classifications that need to be performed, we calculate the separability of the class samples in each CP SAR parameter and select those parameters in which at least two pairs of classes have separability value higher than 1. For the case of Ice and OW, we select those parameters in which the JM

separability value of the ice and the OW is higher than 1. In addition, we set two as the minimum number of parameters in a parameter combination.

EXPERIMENTAL RESULTS AND DISCUSSIONS

Data Set

The simulated CP SAR parameters in Table 1 are calculated from a fine quad-pol RADARSAT-2 SAR image over the Barrow Strait close to Somerset Island in the Canadian Arctic. The data were collected in May 5th, 2010, with incidence angle range between 30.3 and 32.0 degrees and a pixel-spacing of approximately five meters. Sea ice experts form the Canadian Ice Service (CIS) identified three main classes in the selected study area: 1) First Year Ice (FYI), 2) Multi Year Ice (MYI) and Open Water (OW). Figure 1 shows the RGB (R = HH-VV, G = 2HV, B = HH+VV) image of the study area with the selected by the CIS training (solid polygons) and testing (empty polygons) samples. The bottom of the study area contains a land portion which was excluded from the processing using available coastline data. The mean air temperature was -10.4^{o}C and the mean wind speed was 6.1 km/h. Temperature has been < 0^{o}C for months.

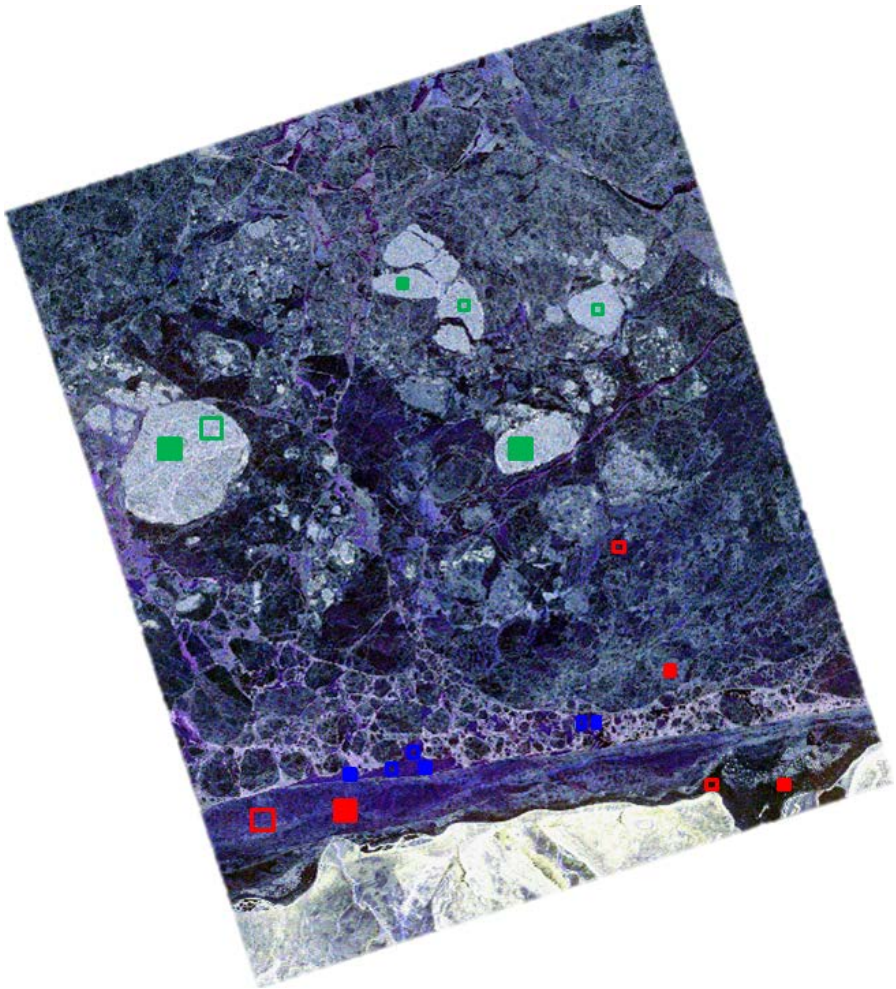

Figure 1. RGB (R = HH-VV, G = 2HV, B = HH+VV) display of the study area with the selected training (solid polygons) and testing (empty polygons) samples.

Jeffries-Matusita (JM) Separability

For each RCM mode, we calculate the JM separability between all possible pairs of classes and the overall mean JM separability in each CP SAR parameter. Furthermore, we also calculate for each CP parameter the separability of the ice as one class versus the OW. We set a conservative threshold that two classes can be separated

if the JM separability value is greater than 1 in the interval [0, 2]. Table 2 presents the calculated JM separability of the classes within each CP parameter for the RCM modes: LN25, LR22, and MR22.

Table 2: The JM separability between the classes FYI, MYI, and OW and the Ice versus OW for the RCM LN25, LR22 and MR22 modes.

	FYI - MYI			FYI - OW			MYI - OW			Overall Mean JM Separability			Ice - OW		
	LN25	LR22	MR22	LN25	LR22	MR22	LN25	LR22	MR22	LN25	LR22	MR22	LN25	LR22	MR22
σ°_{RH}	**1.92**	**1.92**	**1.91**	0.14	0.11	0.06	**1.98**	**1.98**	**1.97**	**1.35**	**1.34**	**1.32**	**1.37**	**1.35**	**1.27**
σ°_{RV}	**1.96**	**1.96**	**1.93**	0.49	0.47	0.35	**1.75**	**1.74**	**1.63**	**1.40**	**1.39**	**1.30**	0.76	0.75	0.65
σ°_{RR}	**1.99**	**1.99**	**1.99**	0.27	0.20	0.15	**1.999**	**1.998**	**1.997**	**1.42**	**1.40**	**1.38**	**1.74**	**1.67**	**1.56**
σ°_{RL}	**1.90**	**1.90**	**1.87**	0.18	0.17	0.11	**1.84**	**1.84**	**1.75**	**1.31**	**1.30**	**1.25**	0.89	0.88	0.78
γ_{rvrh}	0.08	0.12	0.08	**1.73**	**1.73**	**1.80**	**1.39**	**1.31**	**1.55**	**1.07**	**1.05**	**1.15**	**1.52**	**1.46**	**1.64**
δ	0.08	0.08	0.12	0.30	0.30	0.21	0.45	0.45	0.51	0.28	0.28	0.28	0.39	0.39	0.41
m	0.30	0.23	0.22	**1.01**	0.91	0.78	**1.76**	**1.34**	**1.15**	**1.03**	0.82	0.71	**1.33**	**1.04**	0.88
u	0.30	0.21	0.22	0.97	0.89	0.68	**1.68**	**1.24**	0.98	0.98	0.78	0.62	**1.24**	0.98	0.74
ρ	0.27	0.24	0.27	**1.04**	0.98	0.77	**1.66**	**1.22**	0.93	0.99	0.81	0.66	**1.26**	1.00	0.76
μ_c	0.25	0.24	0.27	**1.09**	**1.03**	0.83	**1.65**	**1.25**	1.00	1.00	0.84	0.70	**1.29**	**1.05**	0.82
m-χ-e	**1.29**	**1.29**	**1.40**	**1.33**	**1.33**	**1.48**	0.24	0.24	0.34	0.95	0.95	**1.07**	0.21	0.21	0.29
m-χ-v	**1.995**	**1.99**	**1.99**	0.75	0.60	0.44	**1.9998**	**1.999**	**1.998**	**1.58**	**1.53**	**1.48**	**1.80**	**1.71**	**1.60**
m-χ-o	**1.65**	**1.65**	**1.61**	0.24	0.24	0.17	**1.40**	**1.40**	**1.28**	**1.10**	**1.10**	**1.02**	0.62	0.62	0.52
m-δ-db	**1.18**	**1.18**	**1.37**	0.25	0.25	0.22	**1.49**	**1.49**	**1.61**	0.98	0.98	**1.07**	**1.37**	**1.37**	**1.51**
m-δ-v	**1.995**	**1.99**	**1.99**	0.75	0.60	0.44	**1.9998**	**1.999**	**1.998**	**1.58**	**1.53**	**1.48**	**1.80**	**1.71**	**1.60**
m-δ-s	**1.66**	**1.66**	**1.62**	0.26	0.26	0.20	**1.37**	**1.37**	**1.24**	**1.10**	**1.10**	**1.02**	0.60	0.60	0.50
α-s	0.12	0.12	0.15	0.94	0.94	**1.15**	0.49	0.49	0.59	0.52	0.52	0.63	0.62	0.62	0.76
H_i	**1.89**	**1.91**	**1.89**	0.31	0.24	0.14	**1.95**	**1.95**	**1.91**	**1.38**	**1.37**	**1.31**	0.70	0.70	0.60
H_p	0.31	0.17	0.17	0.77	0.75	0.45	**1.46**	**1.05**	0.73	0.85	0.65	0.45	**1.02**	0.83	0.53
g_0	**1.97**	**1.97**	**1.96**	0.15	0.13	0.08	**1.96**	**1.96**	**1.92**	**1.36**	**1.35**	**1.32**	**1.06**	**1.04**	0.95
g_1	0.78	0.78	0.80	**1.50**	**1.50**	**1.49**	0.61	0.61	0.70	0.96	0.96	1.00	0.65	0.65	0.71
g_2	0.94	0.94	**1.01**	0.10	0.10	0.03	**1.04**	**1.04**	**1.11**	0.69	0.69	0.72	0.86	0.86	0.94
g_3	**1.63**	**1.63**	**1.59**	0.22	0.22	0.15	**1.42**	**1.42**	**1.29**	**1.09**	**1.09**	**1.01**	0.65	0.65	0.54

As shown in Table 2, thirteen CP parameters separate FYI and MYI in the case of RCM LN25 and LR22 modes. These parameters are the same for the two modes. For the MR22 mode, fourteen CP parameters separate FYI and MYI. These are the same parameters of the LN25 and LR22 modes, with an additional parameter, the third component of the Stokes vector (g2). For the RCM LN25 mode, the highest JM separability value between FYI and MYI is obtained by the volume scattering parameters m-χ-v and m-δ-v. For the RCM LR22 and MR22 modes, the highest JM separability value between FYI and MYI is obtained by two parameters: σ^{0}_{RR} and the volume scattering parameters m-χ-v and m-δ-v. The FYI and OW classes are separated by six parameters in the LN25 mode and four parameters in the LR22 and MR22 modes. In the three modes, the ratio γ_{rvrh} provides the highest JM separability value. The MYI and OW classes are separated by nineteen CP parameters in the RCM LN25 and LR22 modes. Fifteen CP parameters are able to separate MYI and OW in the RCM MR22 mode. In the three modes, the volume scattering parameters m-χ-v and m-δ-v provide the highest JM separability value. However, the σ^{0}_{RR} parameter also exhibits very high separability values in the three modes. Among the three modes the highest separability between FYI and MYI is obtained in the LN25 mode (1.995 by the volume parameters). The highest JM separability value between FYI and OW is given in the MR22 mode (1.80 by the ratio γ_{rvrh}). For the classes MYI and OW, the highest JM separability value is obtained in the RCM LN25 mode (1.9998 by the volume parameters).

Based on the overall mean JM separability, the three class combinations are discriminated in thirteen CP parameters for the case of RCM LN25 mode, twelve CP parameters for the case of RCM LR22 mode, and fourteen CP parameters for the case of RCM MR22 mode. Among the three modes, the highest JM separability (1.53) is obtained in the RCM LN25 and LR22 modes by the volume scattering parameters m-χ-v and m-δ-v. The ratio γ_{rvrh} provides the lowest JM separability value for all the three modes (0.28).

The separation between the class Ice and OW is achieved with twelve, nine and six CP parameters in the RCM LN25, LR22, MR22 modes, respectively. The highest separability between Ice and OW is achieved by the volume scattering parameters m-χ-v and m-δ-v in the RCM LN25 and LR22 modes. However, in the RCM MR22 mode, the ratio γ_{rvrh} gives the highest separability between Ice and OW. It is worth to mention that by increasing the noise level and the spatial resolution, the number of the CP parameters which separate Ice and OW is decreasing.

The RCM LN25 mode is compared with the RCM LR22 and RCM MR22 modes to assess the influence of an increased noise level and a higher resolution (Fig. 2). For the overall mean JM separability (Fig. 2a), a general effect is a reduction in separability with an increased noise level and a further reduction with higher resolution. This is most obvious for the m, u, ρ, μ_c and H_p parameters. Small increases in separability are observed with higher resolution for γ_{rvrh}, m-χ-e, m-δ-db, and α-s. For JM separability of Ice and OW (Fig. 2b), the same general reduction in separability is observed with an increased noise level and higher resolution. Similar small increases in separability are observed with higher resolution for γ_{rvrh}, m-χ-e, m-δ-db, and α-s, and also g2.

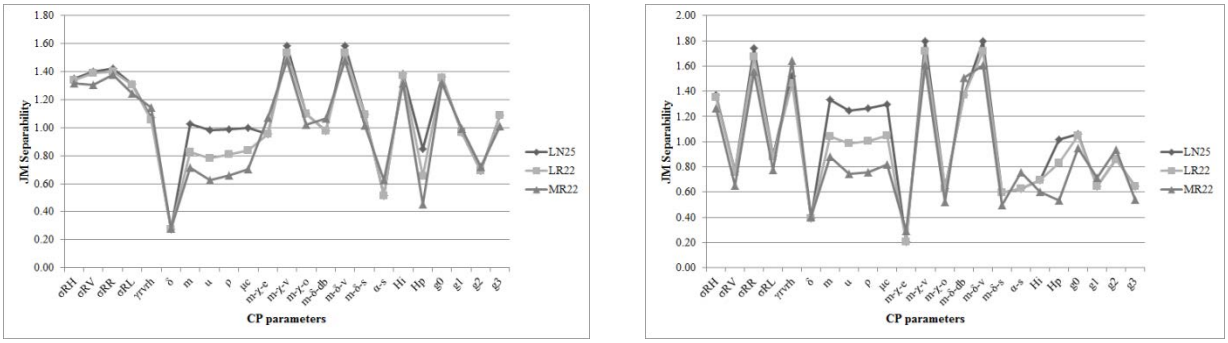

(a) (b)

Figure 2. (a) The overall mean JM separability of the three pairs of classes and (b) The JM separability between the Ice and the OW in the simulated CP SAR parameters for the three RCM modes.

Maximum Likelihood Classification

The calculated CP SAR parameters in each RCM mode are highly correlated. In order to determine those CP parameters needed to obtain the maximum classification accuracy, we apply the ML classification approach using all the possible subsets of the CP parameters and calculate the overall classification accuracy for each classification result. As mentioned previously, in order to reduce the high number of classifications that need to be performed, we use the JM separability to select those CP parameters where at least two class pairs are separable. For the case of Ice versus OW, we select the CP parameters where Ice and OW are separable. We considered two as the minimum number of CP parameters in a subset. We state that the optimal subset is the one which provides the highest overall classification accuracy.

A. The RCM LN25 Mode

Based on the calculated JM separability values (Table 2), seventeen parameters are selected for the ML classification of the FYI, MYI and OW. The highest overall classification accuracy is obtained with the CP subset of two parameters, the ratio γ_{rvrh} and the volume scattering parameter m-χ-v or m-δ-v. Note that the ratio γ_{rvrh} is a CP parameter which separates the OW from the FYI and the MYI, while the volume scattering parameter separates the MYI form the FYI and the OW. Also, the ratio γ_{rvrh} is the CP parameter with the highest JM separability value between the FYI and the OW, while the volume parameter has the highest JM separability value between the classes FYI and MYI and the classes MYI and OW. The overall classification accuracy obtained by these two parameters is equal to 99.92% with a Kappa coefficient value of 0.9985.

We repeat the same batch classification procedure for the classification of Ice and OW. As shown in Table 2, Ice and OW are separable in twelve CP parameters, which are used as input data in the classification approach. The highest obtained overall classification accuracy is equal to 100%. This accuracy is achieved using the four CP parameters: σ^0_{RH}, σ^0_{RR}, γ_{rvrh}, and the volume scattering parameter m-χ-v or m-δ-v. However, the estimation of the importance of each parameter in the achieved overall classification is needed. Thus, for a number of parameters in a subset higher than two, we apply a leave-one-out (LOO) test. Based on the LOO test, we reapply the classification process using n – 1 parameters, where n is the number of CP parameters that provides the highest overall classification accuracy (n > 2). The classification procedure is repeated n times, excluding each time one CP

parameter and calculating the overall classification accuracy. The importance of each CP parameter is associated with its contribution to the overall classification accuracy. This importance/contribution can be evaluated by calculating the reduction in the overall classification accuracy caused by the exclusion of that parameter. Consequently, the higher the reduction is the higher the importance of the excluded CP parameter. We apply the LOO test on the obtained CP subset for Ice and OW. Table 3 shows the CP parameters sorted based on their importance in the classification accuracy.

Table 3: The subset CP parameters for the classification of Ice and OW sorted based on their contribution to the highest overall classification accuracy.

Excluded CP parameter	Overall classification accuracy (%)	Difference from the highest overall accuracy (%)
γ_{rvrh}	85.85	14.15
σ^0_{RR}	99.02	0.98
m-χ-v or m-δ-v	99.41	0.59
σ^0_{RH}	99.62	0.38

As shown in Table 3, the ratio γ_{rvrh} plays crucial role in the discrimination between Ice and OW. Excluding this CP parameter reduces dramatically the overall classification accuracy from 100% to 85.85%. On the other hand, the σ^0_{RH} parameter appears to play minor role in the overall highest classification accuracy, since the exclusion of this parameter causes the smallest reduction (from 100% to 99.62%).

B. The RCM LR22 Mode

The pre-mentioned batch ML classification approach is applied for the case of RCM LR22 mode. For the classification of the FYI, MYI and OW, fifteen CP SAR parameters are used as input data in the classification approach. The highest overall classification accuracy is obtained with a subset of three CP parameters: σ^0_{RH}, γ_{rvrh}, and the fourth Stokes component g3. The obtained highest overall classification based on this subset is equal to 99.47% with Kappa coefficient equal to 0.9906.

We apply the LOO test in order to evaluate the importance of each CP parameter of the resulting subset in the overall highest classification accuracy. Table 4 shows the CP parameters sorted based on their importance in the classification accuracy. As shown in Table 4, the σ^0_{RH} is the parameter with the highest contribution in the overall accuracy. The exclusion of this parameter from the obtained subset reduces the highest overall classification accuracy by 3.98%.

Table 4: The subset CP parameters for the classification of the FYI, MYI, and OW sorted based on their contribution to the highest overall classification accuracy.

Excluded CP parameter	Overall classification accuracy (%)	Difference from the highest overall accuracy (%)
σ^0_{RH}	95.49	3.98
γ_{rvrh}	97.28	2.19
g3	98.18	1.29

The batch classification process is repeated for the classification of the two classes Ice and OW. From Table 2, Ice and OW are separable in nine CP parameters. The highest overall classification accuracy is obtained by a subset of four CP parameters: σ^0_{RR}, γ_{rvrh}, m-χ-v or m-δ-v, and g0. This subset provides overall classification accuracy equal to 99.76%. The LOO test is applied in order to evaluate the importance of the CP parameters of the resulting subset. Table 5 presents the CP parameters sorted based on their importance to achieve the highest overall classification accuracy.

As for the case of the RCM LN25 mode, the ratio γ_{rvrh} is crucial for the discrimination between the ice and the OW in the RCM LR22 mode. The exclusion of this parameter drops greatly the highest overall classification accuracy from 99.76% to 89.60%. This should be associated with the discrimination capability of the ratio γ_{rvrh} between FYI and OW. The rest of the CP parameters have a minor contribution is the highest overall classification accuracy since their exclusion reduces slightly the classification accuracy.

Table 5: The subset CP parameters for the classification of Ice and OW sorted based on their contribution to the highest overall classification accuracy.

Excluded CP parameter	Overall classification accuracy (%)	Difference from the highest overall accuracy (%)
γ_{rvrh}	89.60	10.16
σ^0_{RR}	98.41	1.35
m-χ-v or m-δ-v	98.50	1.26
g0	99.27	0.49

C. The RCM MR22 Mode

Based on Table 2, fifteen CP parameters are used as input data in the batch process for the classification of FYI, MYI and OW. We found that the highest overall classification accuracy is obtained by a subset of ten CP parameters. Herein, the calculated highest overall classification accuracy is equal to 99.44%. In comparison to the previous two RCM modes, we note that the number of CP parameters required to achieve the highest overall classification accuracy is quite higher. The optimal subset contains the CP parameters: σ^0_{RV}, σ^0_{RR}, σ^0_{RL}, m-χ-e, m-δ-db, m-δ-s, H_i, g0, g3, and m-χ-v or m-δ-v. It should be mentioned that the parameter σ^0_{RV}, which has the highest contribution in the overall classification accuracy for the RCM LR22 mode, is not included in the resulting optimal subset for the case of RCM MR22 mode. Also, the ratio γ_{rvrh}, which plays important role in the overall classification accuracy for the RCM LR25 and LR22 modes, does not belong to the resulting optimal subset of the RCM MR22 mode. We apply the LOO test in order to evaluate the importance of each parameter on the highest overall classification accuracy. Table 6 shows the CP parameters sorted based on their importance on the highest overall classification accuracy.

Table 6: The subset CP parameters for the classification of the FYI, MYI, and OW sorted based on their contribution to the highest overall classification accuracy.

Excluded CP parameter	Overall classification accuracy (%)	Difference from the highest overall accuracy (%)
H_i	50.88	48.56
σ^0_{RV}	89.80	9.64
m-χ-e or m-δ-db	96.52	2.92
σ^0_{RR}	97.18	2.26
g0	97.20	2.24
g3	97.52	1.92
m-δ-db	97.63	1.81
m-χ-e	97.97	1.47
σ^0_{RL}	98.43	1.01
m-δ-s	99.24	0.20

As shown in Table 13, the intensity component of the Shannon entropy has crucial impact on the highest overall classification accuracy. The exclusion of this CP parameter dramatically reduces the achieved highest overall classification accuracy from 99.44% to 50.88%. Also, Table 6 indicates that the σ^0_{RV} is the second important parameter. Essential reduction (9.64%) in the highest overall classification accuracy is occurred by the exclusion of this parameter from the obtained CP parameter subset. The lowest impact is associated with the surface parameter of the m-δ decomposition (m-δ-s). The exclusion of this parameter reduces the highest overall classification accuracy by 0.20%.

As shown in Table 2, only six CP parameters are eligible for the batch ML classification process of Ice and OW. The highest overall classification accuracy (99.80%) is obtained by a subset of three CP parameters: σ^0_{RH}, σ^0_{RR}, and γ_{rvrh}. It should be noted that the resulting three optimal subsets of the three RCM modes for the optimal classification of Ice and OW have in common two CP parameters, the σ^0_{RR} and the ratio γ_{rvrh}. The LOO test is applied in order to evaluate the importance of each CP parameter. Table 7 presents the CP parameters sorted based on their importance to achieve the highest overall classification accuracy.

Table 7: The subset CP parameters for the classification of Ice and OW sorted based on their contribution to the highest overall classification accuracy.

Excluded CP parameter	Overall classification accuracy (%)	Difference from the highest overall accuracy (%)
γ_{rvrh}	72.16	27.64
σ^0_{RH}	99.60	0.20
σ^0_{RR}	99.70	0.10

As for the case of the RCM LR25 and LR22 modes, the ratio γ_{rvrh} plays important role in the classification of Ice and OW. The exclusion of this parameter in the RCM MR22 mode greatly reduces the highest classification accuracy by 27.64%. The σ^0_{RH} and σ^0_{RR} parameters appear to have minor contribution in the highest overall classification accuracy, since the exclusion of these two parameters reduces the accuracy by 0.20% and 0.10%, respectively. Note also that the importance of the ratio γ_{rvrh} for the classification of Ice and OW in the RCM MR22 mode is higher than the RCM LR25 and LR22 modes. This is because the exclusion of this CP parameter from the classification process in the RCM MR22 mode produces the lowest overall classification accuracy of Ice and OW (72.16%).

CONCLUSIONS

Twenty three simulated compact polarimetry parameters are evaluated for their classification potential in a sea ice and open water environment, for three RCM modes. A case study is used to identify: 1) parameters with effective Jeffries-Matusita separability; and 2) optimal CP parameters subsets, using batch ML classification. The JM separability of most CP parameters is decreased with an increase in noise level, as well as with higher resolution. However, the increased noise level and higher resolution have little impact on the ML classification accuracy. The high accuracies of the classifications in this case study suggest that the methodology is effective at identifying the optimum CP parameter subsets, and that these CP parameter subsets are effective at classifying sea ice and open water. Further testing is required at other incidence angles, for additional sea ice types and conditions, and for a range of open water states.

ACKNOWLEDGEMENTS

We thank F. Charbonneau at the Canada Centre for Remote Sensing for supplying the RCM simulator, and T. Zagon at the Canadian Ice Service for image interpretation. Dr. Dabboor's visiting fellowship at Environment Canada is supported with funding from the Canadian Space Agency's Government Related Initiatives Program. RADARSAT-2 Data and Products (c) MacDonald, Dettwiler and Associates Ltd., 2010 - All Rights Reserved.

REFERENCES

Charbonneau, F.J., B. Brisco, R.K. Raney, H. McNairn, C. Liu, P. Vachon,J. Shang, R. DeAbreu, C. Champagne, A. Merzouki, and T. Geldsetzer, 2010. Compact polarimetry overview and applications assessment, *Canadian Journal of Remote Sensing*, *36*(2): S298–S315.

Cloude, S.R., D.G. Goodenough, and H. Chen, 2012. Compact decomposition theory. *IEEE Geoscience and Remote Sensing Letters*, *9*(1): 28-32.

Duda, R., Hart, P., and Stork, D., 2000. *Pattern classification*, Wiley, New York, pp. 3-33.

Geldsetzer, T., and J.J. Yackel, 2009. Sea ice type and open water discrimination using dual co-polarized C-band SAR, *Canadian Journal of Remote Sensing*, *35*(1): 73-84.

Gill, J.P., and J.J. Yackel, 2012. Evaluation of C-band SAR polarimetric parameters for discrimination of first-year sea ice types, *Canadian Journal of Remote Sensing*, *38*(03): 306-323.

Raney, R. K., 2007. Hybrid-polarity SAR architecture, *IEEE Transactions on Geoscience and Remote Sensing*, *45*(11): 3397–3404.

Raney, R. K., J. T. S. Cahill, G. W. Patterson, and D. B. J. Bussey, 2012. The m-chi decomposition of hybrid dual-polarimetric radar data with application to lunar craters, *Journal of Geophysical Research*, *117*(E12): 1-8.

Richards, J. A., 1999. *Remote sensing digital image analysis: an introduction*, Fifth edition, Springer-Verlag, Berlin.

Swain, P. H. and Davis, S. M., 1978. *Remote Sensing: the quantitative approach*, McGraw-Hill, New York.

Truong-Loi, M., A. Freeman, P. Dubois-Fernandez, and E. Pottier, 2009. Comparison between the conformity coefficient and previous classification techniques for bare surface discrimination and application to compact polarimetry mode. *Proceedings of 4th International Workshop on Science and Applications of SAR Polarimetry and Polarimetric Interferometry – PolInSAR 2009*, January 26-30, 2009.